Jianfei Wang
Institute of Metal Research,
Chinese Academy of Sciences,
Shenyang 110016, China;
School of Materials Science and Engineering,
University of Science and Technology of China,
Shenyang 110016, China
e-mail: jfwang17s@imr.ac.cn

Weihai Xue[1]
Institute of Metal Research,
Chinese Academy of Sciences,
Shenyang 110016, China
e-mail: whxue@imr.ac.cn

Siyang Gao
Institute of Metal Research,
Chinese Academy of Sciences,
Shenyang 110016, China
e-mail: sygao@imr.ac.cn

Bi Wu
Institute of Metal Research,
Chinese Academy of Sciences,
Shenyang 110016, China;
School of Materials Science and Engineering,
University of Science and Technology of China,
Shenyang 110016, China
e-mail: bwu17b@imr.ac.cn

Shu Li
Institute of Metal Research,
Chinese Academy of Sciences,
Shenyang 110016, China;
School of Materials Science and Engineering,
University of Science and Technology of China,
Shenyang 110016, China
e-mail: shuli@imr.ac.cn

Deli Duan[1]
Institute of Metal Research,
Chinese Academy of Sciences,
Shenyang 110016, China;
School of Materials Science and Engineering,
University of Science and Technology of China,
Shenyang 110016, China
e-mail: duandl@imr.ac.cn

System Deformation Behavior of Friction Pair in Fretting Wear

Several criteria for fretting wear behavior evaluation have been established since the proposal and establishment of the fretting loop concept. In this article, system deformation and system deformation ratio were defined. In addition, the fretting running conditions were distinguished from the evolution of system deformation with fretting cycles during fretting wear tests under different applied displacements and loads. In the gross slip regime, the system deformation was independent of the applied displacement and increased as the load increased, whereas in the partial slip regime, the system deformation was independent of the load and increased with the applied displacement. Furthermore, a linear relationship between the system deformation and the applied load in gross slip regime was found for the first time. Based on this linear relationship, the system deformation ratio can forecast the running regime with a given load and displacement. For the titanium alloy fretting pairs studied in this article, the fretting wear was found to run in the gross slip regime if the system deformation ratio was smaller than 0.9. Based on these observations, the system deformation ratio exhibited applicability in assisting the mechanical design of equipment suffering from fretting wear. [DOI: 10.1115/1.4047951]

Keywords: fretting wear, gross slip, partial slip, fretting regime prediction, fretting wear model, dry friction, stick-slip, tribological systems, wear, wear mechanisms

1 Introduction

Titanium alloy has become an indispensable material in the aerospace industry because of its excellent comprehensive properties, such as its high specific strength, wide temperature range, and good corrosion resistance. However, titanium alloy has poor resistance to fretting wear [1,2]. Fretting wear is a form of damage that prevails in the nominal relative static mechanical pairs and is caused by the micro-scale vibration under the normal load [3]. The working life of the compressor blade in the aircraft engine is greatly reduced by fretting wear due to the high-frequency vibration, which is a great hidden danger [4].

Since Mindlin first studied contact mechanics of spheres under tangential loading [5], several fretting wear models have been proposed in the last six decades [6,7]. However, early studies were limited by the test conditions and the level of awareness of fretting wear, such that the fretting wear models were not thoroughly satisfactory. Uhlig [8] quantitatively reported the theoretical expression of the material loss in fretting wear although the study only mildly considered the wear debris and partial slip regime. The third-body effect was only thoroughly investigated in 1984 [9]. Since then, the third-body effect has received the attention it deserves, and later studies revealed the role of debris [10–14].

The proposal of the fretting loop (tangential force–displacement curve) introduced the practicality and applicability of the fretting models. Fouvry et al. [15–17] proposed the relationship between the dissipated energy and the wear volume in fretting wear. The area of the closed fretting loop curve was defined as the dissipated energy during a fretting cycle. A unified energy wear formulation was then put forward, which could describe both the nonadhesive and adhesive wear interfaces. Heredia and Fouvry [18] introduced the % gross slip (%GS), which was defined as the proportion of

[1]Corresponding authors.
Contributed by the Tribology Division of ASME for publication in the JOURNAL OF TRIBOLOGY. Manuscript received May 8, 2020; final manuscript received June 28, 2020; published online August 14, 2020. Assoc. Editor: Yong Hoon Jang.

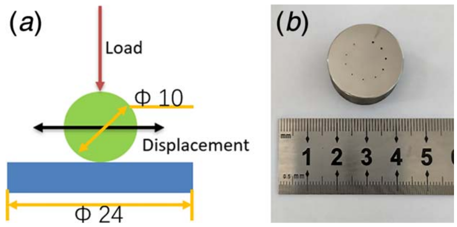

Fig. 1 (a) Illustration of the ball-on-flat specimen configuration applied in the fretting tests and (b) the lower sample

cycles running in the GS regime to the total cycles. With the help of % GS, the partial slip regime, mixed regime, and gross slip regime could be quantitatively distinguished. Fouvry et al. [19] studied the sliding ratio (D) to quantify the fretting behavior based on the Mindlin hypotheses. The theoretical derivation and test results indicated a transition of $D = 0.26$ from partial slip to gross slip. Varenberg et al. [20] presented a unified approach to fretting based on a dimensionless parameter, namely, the slip index, wherein reciprocal sliding was observed at slip indexes larger than 11. Similarly, gross slip was characterized between 0.8 and 10, whereas partial slip was characterized between 0.5 and 0.6. However, the complex slip index calculations required initial fretting loop drawings and elastic loop slope measurements prior to calculations. Wang et al. [21] defined fretting scar diameter ratio (α) to characterize fretting running conditions based on the wear of the paired samples. If α was less than 1.2, it meant that the fretting was in the partial slip regime; otherwise, it was in the gross slip regime.

In recent years, wear in the fretting process has been commonly modeled on the finite element method (FEM) due to its efficiency and applicability [7,22,23]. With the help of FEM, the effects of roughness [24], debris [14,22], and coefficient of friction (COF) [25] have been revealed during the fretting wear process. Pereira et al. [24] presented a multiscale methodology to consider the roughness effect in fretting wear simulations and found that roughness minimally affected the normal load under fretting wear in a gross sliding condition. Yue et al. [14] developed a plane strain fretting wear model with a debris layer to investigate the effects of debris on the fretting wear damage. The results indicated that at the beginning of the fretting wear cycles, the debris layer protected the contact surface and reduced the wear volume compared to the results of the model without the debris layer. In addition, after 18,000 cycles, more wear damage was observed when considering the effects of the debris layer. Yue et al. [25] studied the effect of the variable COF in gross sliding and partial slip conditions on fretting wear. The results showed that in the gross sliding condition, a variable COF had little effect during the steady-state stage but presented a larger effect in the partial slip or running-in stage of gross sliding.

Unfortunately, neither the models acquired from experimental tests nor the FEM models could predict the fretting running conditions without testing, which is generally very helpful for the mechanical design. For example, a designer could initiate the mechanical parts to run in a preferred fretting condition based on the working conditions of the prediction model. In this article, we conducted an in-depth study on the fretting wear with a ball-on-flat contact geometry of the Ti-6Al-4V alloy at a high frequency of 100 Hz. The system deformation and system deformation ratio were proposed based on the fretting loops. The given load and the displacement results aided in the prediction of the fretting running conditions.

2 Experiment

2.1 Materials and Test Procedures. The experiment adopted a ball-on-flat geometry (Fig. 1(a)), wherein the upper sample was a ball and the lower sample was a plate (Fig. 1(b)). In this article, both the ball and plate samples were composed of the Ti-6Al-4V alloy. The upper ball specimen exhibited a radius of 5 mm. The lower cylindrical plate presented a radius of 12 mm and a thickness of 8 mm, such that at least ten were conducted on the lower plate sample (Fig. 1(b)). Prior to the experiment, the lower specimen was ground with sandpaper with roughness grades of No. 600, No. 800, No. 1000, No. 1200, No. 1500, and No. 2000 and then polished with a SiO_2 polishing solution for 20 min. Prior to the test, the ball and the plate samples were placed in acetone and ultrasonically cleaned for 15 min.

The test equipment is the Rtec fretting machine (Fig. 2). The left and right cylinder parts represent two large thrust high-frequency electromagnetic drive motor transmissions. Driven by the electromagnetic motor, the upper ball specimen carried by a rigid cantilever beam was able to make small displacement reciprocating motions. The reciprocating displacement was monitored by an linear variable differential transformer (LVDT) sensor with a resolution of 0.1 μm. The vertical load was applied on the upper ball specimen through a spring by a servo motor. When loading, a deflection was observed on the right end of the cantilever beam and the upper ball was pressed on the lower plate. At this time, the F_z sensor recorded the load and returned the feedback to the loading servo motor.

The frequency was maintained constant at 100 Hz for 100,000 cycles. According to the Hertz contact stress formula and the mechanical property of the Ti-6Al-4V alloy [5,26], the load-generating material yielded at a spherical/plane contact of 120 N. Therefore, to study the influence of the load, the contact stress was controlled within the elastic limit of the material, and the loads were set to 15 N, 20 N, 30 N, 40 N, 50 N, 60 N, 70 N, 80 N, 90 N, and 100 N. The displacements were set to 20 μm, 30 μm, 40 μm, and 50 μm. Two equivalent tests were conducted under each test parameter. After the tests, fretting loops under cycle number 4500,

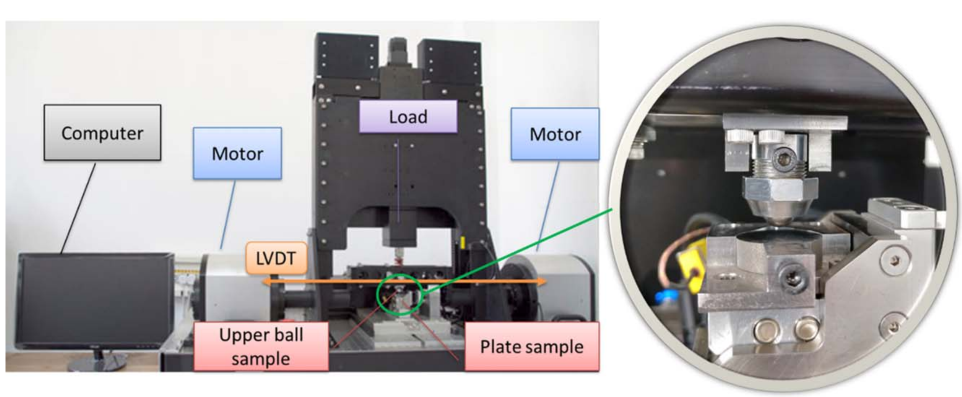

Fig. 2 Schematic of the Rtec fretting machine

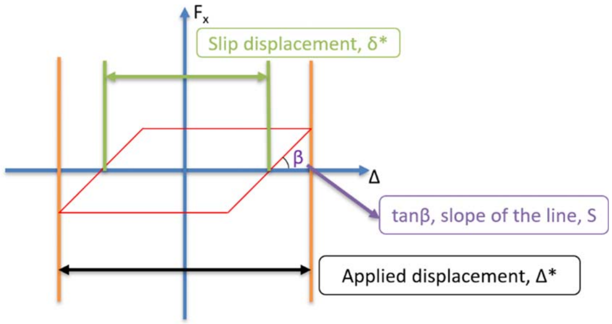

Fig. 3 Schematic diagram of the three parameters in the fretting loop

14,500, 24,500, 34,500, 44,500, 54,500, 64,500, 74,500, 84,500, and 94,500 were drawn under each test parameter. The system deformations were then calculated from the fretting loops.

2.2 Introduction of System Deformation. Several basic parameters were previously defined for a typical fretting loop [27]. As shown in Fig. 3, Δ^* represents the applied displacement in the test, δ^* represents the actual contact slip displacement between the specimens, Δ and F_x represent the continuous recording displacement and load during the whole test, and S is the slope of the line and represents the stiffness of the system. In this article, the deviation between the applied displacement and the slip displacement was defined as the system deformation δ_s, which could be calculated by

$$\delta_s = \Delta^* - \delta^* \tag{1}$$

In other words, the applied displacement (Δ^*) was realized by two parts in each fretting test, namely, through the slip displacement (δ^*) and system deformation (δ_s).

System deformation is a physical quantity that can reflect the extent of material deformation in a fretting loop. For example, as shown in Eq. (1), a larger system deformation indicates a smaller slip displacement when the applied displacement remained constant. As a consequence, adhesion area increased. In other words, the system deformation can reflect the relationship between the slip and stick, as well as between the gross slip regime and the partial slip regime.

3 Results

Figure 4 shows the evolution of system deformation with the fretting cycles under different test parameters. In Fig. 4 (20 μm), the aforementioned seven curves (loads from 40 N to 100 N) were combined together. Associated with the images of the top view of the fretting wear scars (Fig. 5), it was indicated that a load greater than 30 N presented sticking in the central region of the wear scar and only the edge region experienced sliding wear. These observations indicated that fretting was in the partial slip regime. According to Fig. 5, under the resting loads of 15 N, 20 N, and 30 N, the whole contacting area experienced wear, indicating that the fretting was under the gross slip regime. The sticking phenomenon was also observed in the central region of the wear scar under the applied displacements of 30 μm and 40 μm, which correspond to the load reaching 70 N and 90 N, respectively (marked with a dotted box in Fig. 4 (30 μm and 40 μm)). Based on these observations, fretting was concluded to run in the partial slip regime when the system deformation remained invariable with the increased loads.

At an applied displacement of 50 μm, a sticking region was not observed in the wear scars tested under different loads ranging from

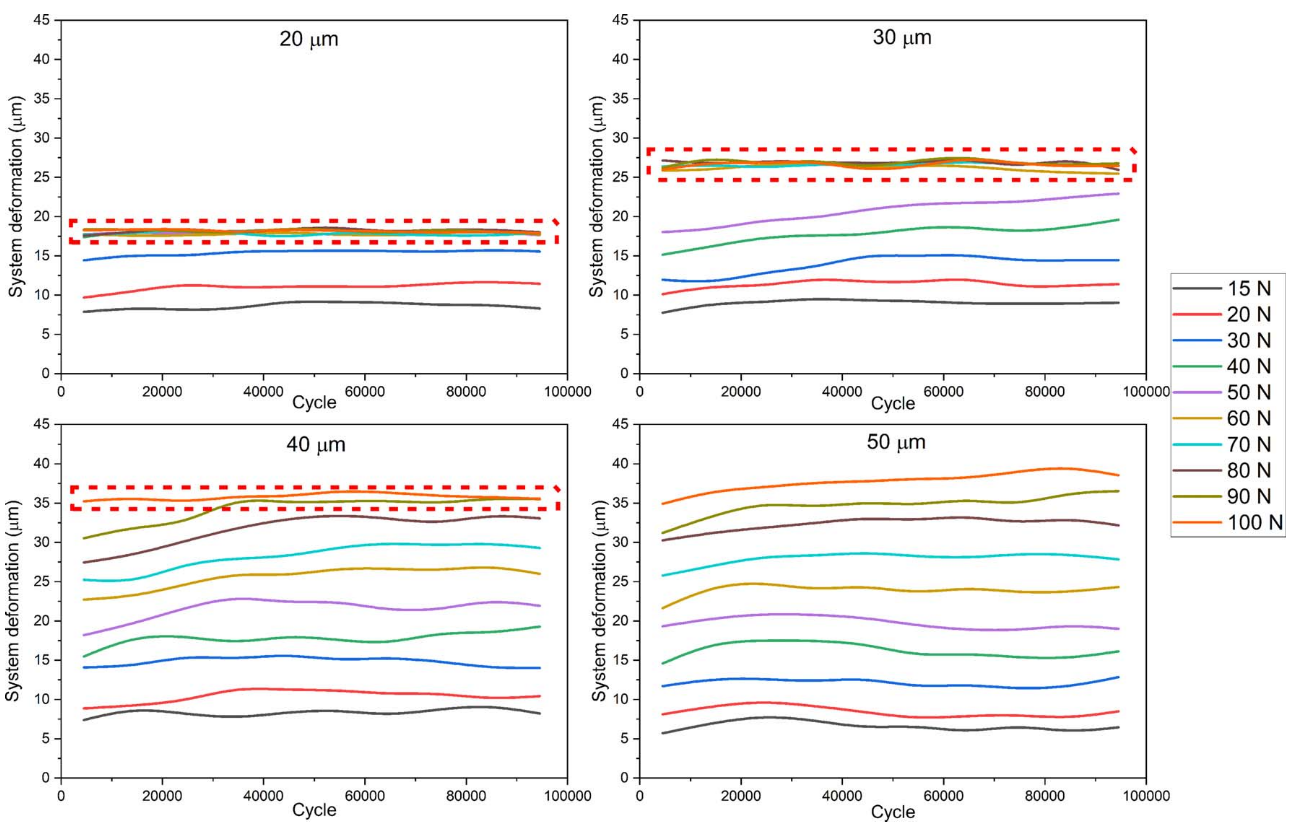

Fig. 4 Evolutions of system deformation under different loads ranging from 15 N to 100 N under the applied displacements of 20 μm, 30 μm, 40 μm, and 50 μm when rubbed with a Ti-6Al-4V ball

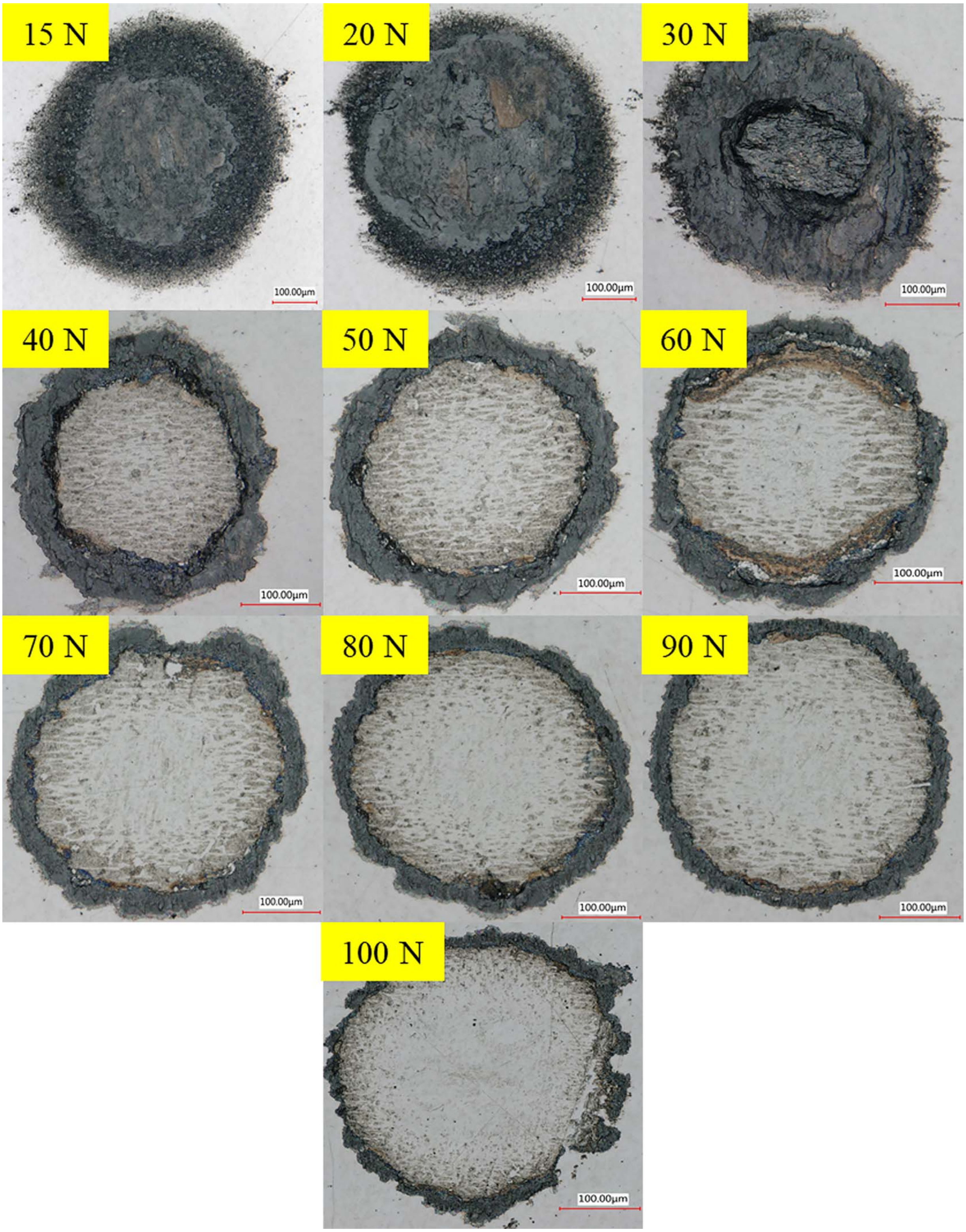

Fig. 5 Top view images of the fretting wear scar under an applied displacement of 20 μm

15 N to 100 N (Fig. 6). Correspondingly, the system deformation increased evenly with the loads (Fig. 4 (50 μm)). However, for the fretting run in the mixed fretting regime, the shape of the fretting loops changed as the fretting cycles changed, suggesting that the system deformation also changed with the fretting cycles. According to Fig. 4, under some test parameters, specifically 20 μm/30 N, 30 μm/50 N, and 40 μm/90 N, the system deformation increased at the beginning and then stabilized as the fretting cycles increased. These observations indicated that the stick and slip state changed during the test, and these test conditions generated fretting runs in the mixed fretting regime. As a result, the partial slip regime, mixed fretting regime, and gross slip regime were easily distinguished from the system deformation evolutions under different loads.

According to Fig. 4, after approximately 50,000 cycles, the system deformation remained somewhat constant with the fretting cycles. Therefore, the system deformations of the last 50,000

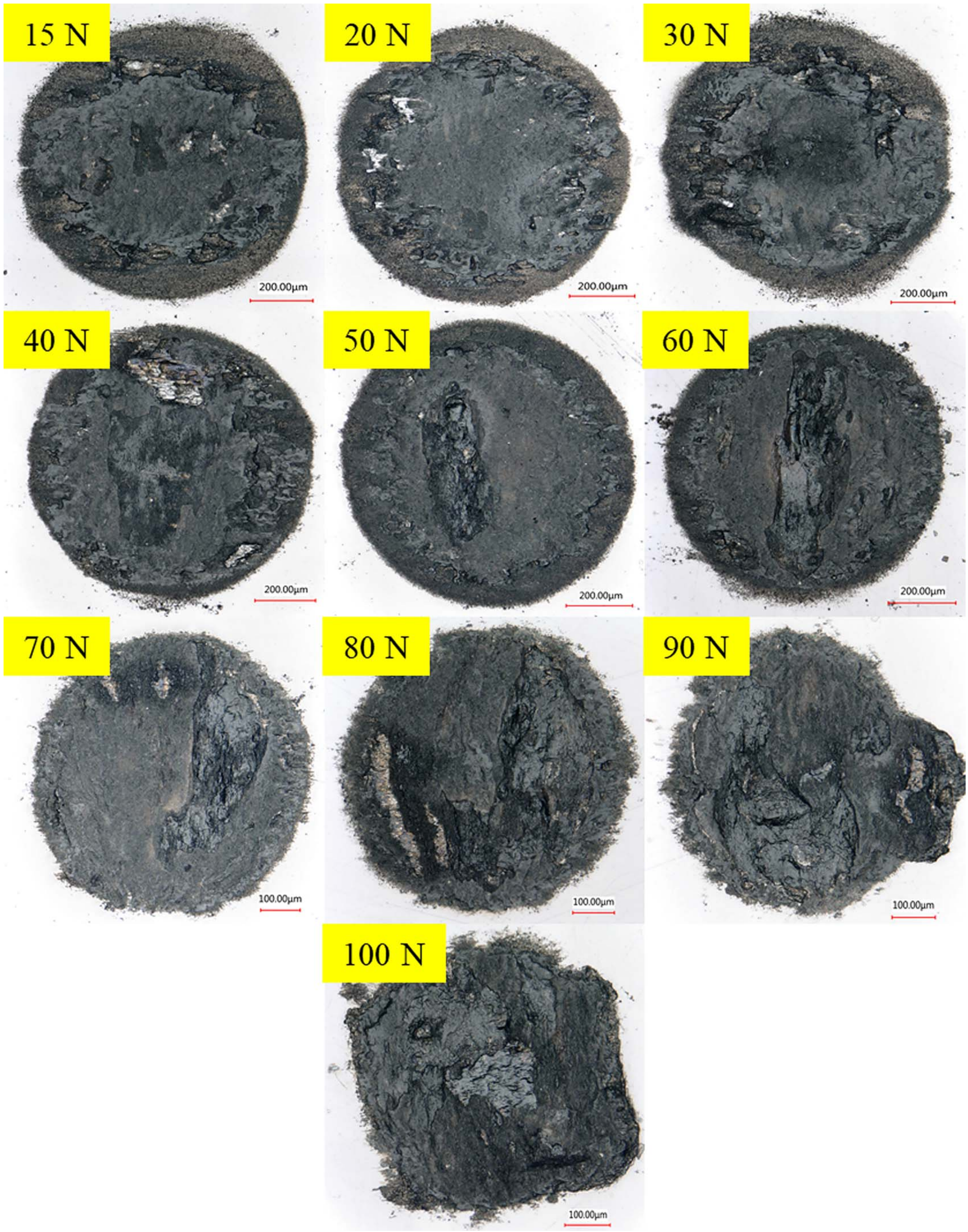

Fig. 6 Top view images of the fretting wear scar under an applied displacement of 50 μm

cycles in each test were averaged to be the system deformation of this test; all of the averaged system deformations are shown in Fig. 7. According to Fig. 4, the gathered points in Fig. 7 represented the tests running in the partial slip regime. Conversely, the scattered points in Fig. 7 corresponded to the tests in the gross slip regime. In the mixed fretting regime, the system deformation also stabilized as the fretting cycles changed, and the stable state entered either partial slip or gross slip, and the mixed fretting regime was no longer separately discussed. It could be found that, in the gross slip regime, the system deformation was mainly dependent on the applied load and the applied displacement has little effect. The system deformation increased as the load increased.

When the applied displacement was constant, the fretting running conditions changed from the gross slip regime to the partial slip regime as the load increased. In this process, the system deformation first increased and then remained stable. When the fretting

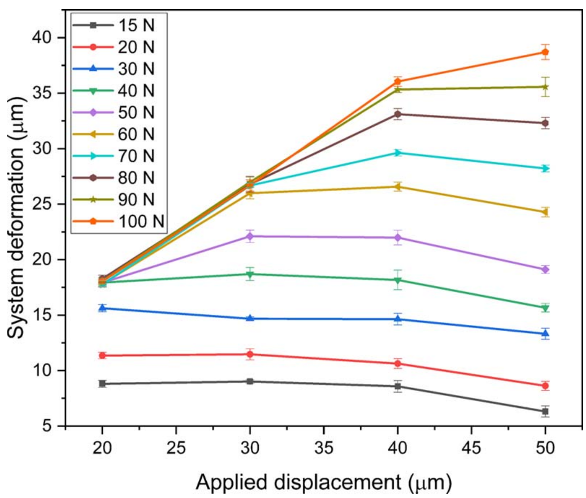

Fig. 7 Evolutions of system deformation with the applied displacements under different loads ranging from 15 N to 100 N when rubbed with a Ti-6Al-4V ball

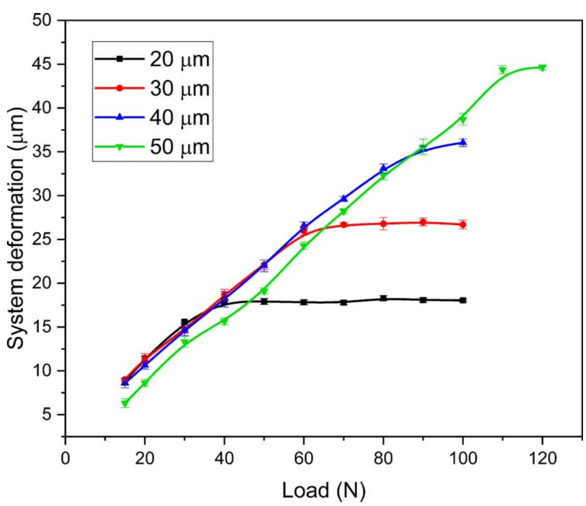

Fig. 8 Evolutions of system deformation with the load under different applied displacements when rubbed with a Ti-6Al-4V ball

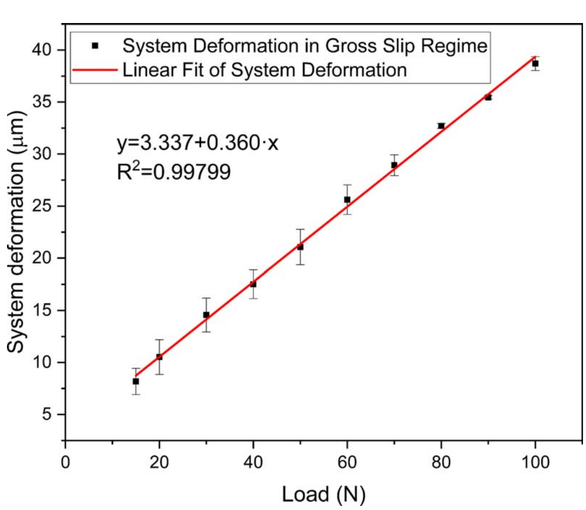

Fig. 9 Average system deformation variation as a function of the load when rubbed with a Ti-6Al-4V ball

Table 1 Summary of the fretting test conditions rubbed with a ceramic ball and a SAE52100 ball

Ball	Si_3N_4	SAE52100
Normal load (F_z) (N)	15, 20, 30, 40, 50, 60, 70, 80, 90, 100	20, 40, 60, 80, 100
Applied displacement (Δ^*) (μm)	40, 50	
Frequency (Hz)	100	
Test duration (cycles)	100,000	

running condition was in the partial slip regime, the system deformation was independent of the load and was only related to the applied displacement, such that the system deformation increased with the applied displacement.

Figure 8 presents the evolutions of system deformation with the load to clearly define the relationship between the system deformation and the load. It could be found that at applied displacements of 20 μm, 30 μm, and 40 μm, the system deformation increased at the initial stage with increasing loads and then stabilized. The critical load under which the system deformation became stable differed with the applied displacement. The system deformation in the steady stage meant that the fretting running condition was in the partial slip regime. However, under an applied displacement of 50 μm, the fretting running condition was still in the gross slip regime even at a load of 100 N. Therefore, extra tests under the loads of 110 N and 120 N were added. The results indicated that the system deformation under an applied displacement of 50 μm also reached a steady value when the load reached 110 N.

The system deformations of the fretting tests running in the slip regime under different applied displacements were averaged given that the system deformation in the gross slip zone was independent of the applied displacement and was only decided by the load. In addition, its relationship with the load is plotted in Fig. 9, wherein the scatter points presented a linear fit.

The system deformation exhibited a very good linear relationship with the load and was defined by the following equation:

$$\delta_s = 3.337 + 0.360 \times F_z \tag{2}$$

where F_z is represented in the units of N and δ_s is represented in the units of μm. The equation was well comprehended that when the load increased, tangential force also increased, which resulted with larger deformation.

4 Discussion

4.1 Fretting Tests on Other Friction Pairs With Different Ball Materials. The fretting wear behaviors were quite different with different friction pair materials [28–31]. To verify the applicability of the system deformation against other materials, extra fretting tests were also performed, wherein the Ti-6Al-4V plate was rubbed with a ceramic ball and a SAE52100 ball. The test conditions are summarized in Table 1.

Following the experimental runs, the data were processed in a similar way to that the method illustrated in Sec. 3. Similar linear relationships were observed when the fretting was run in the gross slip regime (Fig. 10). These observatoins indicated that the linear relationship between the system deformation and the load was also observed in the fretting of the Ti-6Al-4V plate that was rubbed with the ceremic ball and SAE52100 ball.

Interestingly, the slopes of the three fitted lines were almost equal, but the intercepts of the fitted lines differed. This observation indicated that different upper ball materials more significantly influenced the intercept rather than the slope. However, the explicit meaning of the slope and the intercept, as well as their relationship with the friction pair materials, requires further examination.

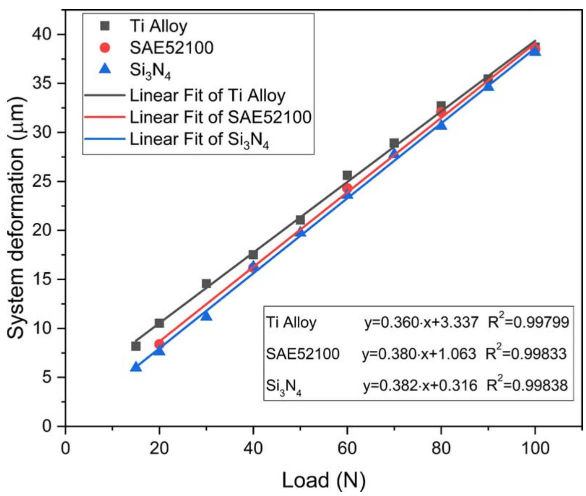

Fig. 10 Average system deformation variation as a function of the load in the gross slip regime, which was rubbed with balls of different materials

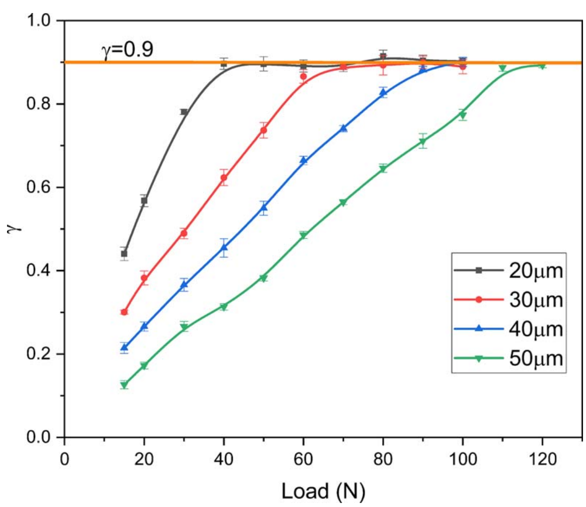

Fig. 11 Evolutions of system deformation ratio with the load under different applied displacements when rubbed with a Ti-6Al-4V ball

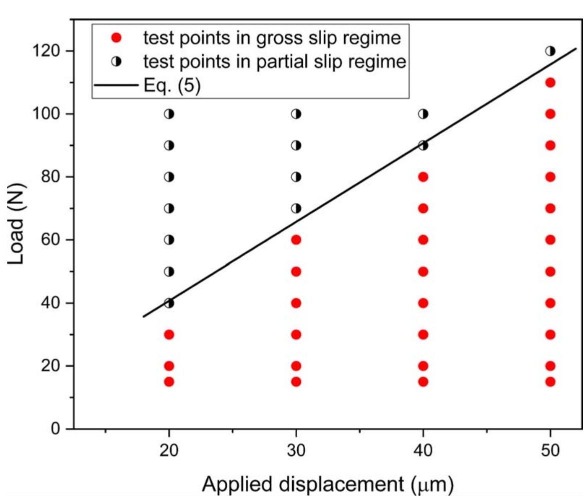

Fig. 12 Curve of Eq. (5), which divided the test parameters under different fretting running conditions into two parts

4.2 System Deformation Ratio as a Criterion for Fretting Running Condition Prediction. As the system deformation was only related to the applied displacement in the partial slip regime, a system deformation ratio was proposed. The system deformation ratio (γ) was defined as the quotient of system deformation and the applied displacement as follows:

$$\gamma = \frac{\delta_s}{\Delta^*} \tag{3}$$

Figure 11 presents the evolutions of the system deformation ratio with the load. The system deformation ratio increased with the load at the initial stage and then remained stable under the applied displacements of 20 μm, 30 μm, 40 μm, and 50 μm. The tested material system exhibited a critical system deformation ratio of 0.9. These results suggest that the fretting running condition was in the gross slip regime when $\gamma < 0.9$. Conditions for all other γ were in the partial slip regime. However, when fretting was in the mixed fretting regime, the system deformation ratio initially changed with the fretting cycles and then remained stable. However, the mixed fretting regime was not discussed in this section given that Fig. 11 only presents the stable value.

The system deformation exhibited dependence on the load in the gross slip regime (Eq. (2)). Combining Eqs. (2) and (3), the system deformation ratio (γ) and the load (F_z) as well as the applied displacement (Δ^*) can be defined as follows:

$$\gamma = \frac{\delta_s}{\Delta^*} = \frac{3.337 + 0.360 \times F_z}{\Delta^*} \tag{4}$$

By using the definition of the experimental conditions, specifically the load and applied displacement, we can forecast the fretting running conditions without additional testing due to their relationship with γ. A γ of less than 0.9 indicated that the fretting running condition under the test parameter was in the gross slip regime; otherwise, it was in partial slip regime. Equating $\gamma = 0.9$ in Eq. (4), the relationship between F_z and Δ^* could be defined as follows:

$$F_z = 2.500 \times \Delta^* - 9.269 \tag{5}$$

The curve of Eq. (5) represents the division of the $F_z - \Delta^*$ coordinate plane into two parts (Fig. 12). The upper left region was executed in the partial slip regime, and the bottom right region was in the gross slip regime. The test points are also drawn in Fig. 12. The tested points in the correct region corresponded well to the fretting running conditions. With the help of Fig. 12, the fretting running conditions of the Ti-6Al-4V alloy/Ti-6Al-4V alloy friction pairs were able to more intuitively and conveniently forecast the conditions.

5 Conclusions

In this study, fretting tests between a Ti-6Al-4V plate and a Ti-6Al-4V ball as well as a ceramic ball and a SAE52100 ball were performed, to which the system deformation concept was proposed. System deformation is a physical quantity that reflects the extent of material deformation in a fretting loop. Based on the system deformation, some conclusions were generated:

- In the gross slip regime, the system deformation was independent of the applied displacement and was only related to the load, such that it increased as the load increased. In the partial slip regime, the system deformation was independent of the load and was only related to the applied displacement, such that it increased with the applied displacement.
- The system deformation in the gross slip regime exhibited a very good linear relationship with the load. The linear relationship was $\delta_s = 3.337 + 0.360 \times F_z$. Notably, the equation was only applicable for Ti-6Al-4V/ Ti-6Al-4V ball-on-flat contact geometry.

- A linear relationship between the system deformation and the applied load was also observed when the Ti-6Al-4V plate was rubbed against a ceramic ball or a SAE52100 ball. The slopes were nearly equal to that of the Ti-6Al-4V ball, yet different intercepts were observed. Further studies are needed to verify the applicability of this linear relationship with other materials.
- The system deformation ratio (γ), which could be calculated with the given normal load (F_z) and applied displacement (Δ^*) when the fretting was running-in gross slip condition, was proposed to predict fretting running conditions. For Ti-6Al-4V/ Ti-6Al-4V ball-on-flat contact geometry, when $\gamma < 0.9$, the fretting running condition was in the gross slip regime; otherwise, it was in the partial slip regime.

Acknowledgment

This project was supported by The Shenyang Key Laboratory of Aero-engine Materials Tribology (SKLAMT201903).

Conflict of Interest

There are no conflicts of interest.

Data Availability Statement

The authors attest that all data for this study are included in the paper. No data, models, or code were generated or used for this paper.

References

[1] Ruiz, C., Boddington, P. H. B., and Chen, K. C., 1984, "An Investigation of Fatigue and Fretting in a Dovetail Joint," Exp. Mech., **24**(3), pp. 208–217.
[2] Hammouda, M. M. I., Pasha, R. A., and Fayed, A. S., 2007, "Modelling of Cracking Sites/Development in Axial Dovetail Joints of Aero-Engine Compressor Discs," Int. J. Fatigue., **29**(1), pp. 30–48.
[3] Gallego, L., and Nélias, D., 2007, "Modeling of Fretting Wear Under Gross Slip and Partial Slip Conditions," ASME J. Tribol., **129**(3), pp. 528–535.
[4] Fridrici, V., Fouvry, S., and Kapsa, P., 2003, "Fretting Wear Behavior of a Cu–Ni–In Plasma Coating," Surf. Coat. Technol., **163–164**, pp. 429–434.
[5] Mindlin, R. D., 1949, "Compliance of Elastic Bodies in Contact," J. Appl. Mech., **16**(3), pp. 259–268.
[6] Meng, H. C., and Ludema, K. C., 1995, "Wear Models and Predictive Equations: Their Form and Content," Wear, **181–183**, pp. 443–457.
[7] Yue, T., and Wahab, M. A., 2019, "A Review on Fretting Wear Mechanisms, Models and Numerical Analyses," CMC Comput. Mat. Contin., **59**(2), pp. 405–432.
[8] Uhlig, H. H., 1954, "Mechanism of Fretting Corrosion," ASME J. Appl. Mech., **21**(4), pp. 401–407.
[9] Godet, M., 1984, "The Third-Body Approach: A Mechanical View of Wear," Wear, **100**(1), pp. 437–452.
[10] Godet, M., 1990, "Third-Bodies in Tribology," Wear, **136**(1), pp. 29–45.
[11] Fillot, N., Iordanoff, I., and Berthier, Y., 2007, "Wear Modeling and the Third Body Concept," Wear, **262**(7), pp. 949–957.
[12] Berthier, Y., 1990, "Experimental Evidence for Friction and Wear Modelling," Wear, **139**(1), pp. 77–92.
[13] Sauger, E., Fouvry, S., Ponsonnet, L., Kapsa, P., Martin, J. M., and Vincent, L., 2000, "Tribologically Transformed Structure in Fretting," Wear, **245**(1), pp. 39–52.
[14] Yue, T., and Wahab, M. A., 2016, "A Numerical Study on the Effect of Debris Layer on Fretting Wear," Materials, **9**(7).
[15] Fouvry, S., Paulin, C., and Deyber, S., 2009, "Impact of Contact Size and Complex Gross-Partial Slip Conditions on Ti-6Al-4V/Ti-6Al-4V Fretting Wear," Tribol. Int., **42**(3), pp. 461–474.
[16] Fouvry, S., Duó, P., and Perruchaut, P., 2004, "A Quantitative Approach of Ti–6Al–4V Fretting Damage: Friction, Wear and Crack Nucleation," Wear, **257**(9), pp. 916–929.
[17] Fouvry, S., Liskiewicz, T., Kapsa, P., Hannel, S., and Sauger, E., 2003, "An Energy Description of Wear Mechanisms and Its Applications to Oscillating Sliding Contacts," Wear, **255**(1), pp. 287–298.
[18] Heredia, S., and Fouvry, S., 2010, "Introduction of a New Sliding Regime Criterion to Quantify Partial, Mixed and Gross Slip Fretting Regimes: Correlation With Wear and Cracking Processes," Wear, **269**(7), pp. 515–524.
[19] Fouvry, S., Kapsa, P., and Vincent, L., 1995, "Analysis of Sliding Behaviour for Fretting Loadings: Determination of Transition Criteria," Wear, **185**(1), pp. 35–46.
[20] Varenberg, M., Etsion, I., and Halperin, G., 2004, "Slip Index: A New Unified Approach to Fretting," Tribol. Lett., **17**(3), pp. 569–573.
[21] Wang, J., Duan, D., Xue, W., Gao, S., and Li, S., 2020, "Ti-6Al-4V Fretting Wear and a Quantitative Indicator for Fretting Regime Evaluation," Proc. Inst. Mech. Eng., Part J.
[22] Wang, S., Yue, T., and Wahab, M. A., 2020, "Multiscale Analysis of the Effect of Debris on Fretting Wear Process Using a Semi-Concurrent Method," CMC Comput. Mat. Contin., **62**(1), pp. 17–35.
[23] Yue, T., and Abdel Wahab, M., 2014, "Finite Element Analysis of Stress Singularity in Partial Slip and Gross Sliding Regimes in Fretting Wear," Wear, **321**, pp. 53–63.
[24] Pereira, K., Yue, T., and Wahab, M. A., 2017, "Multiscale Analysis of the Effect of Roughness on Fretting Wear," Tribol. Int., **110**, pp. 222–231.
[25] Yue, T., and Abdel Wahab, M., 2017, "Finite Element Analysis of Fretting Wear Under Variable Coefficient of Friction and Different Contact Regimes," Tribol. Int., **107**, pp. 274–282.
[26] Hertz, H., 1882, "On the Contact of Elastic Solids," J. Reine Angew. Math, **92**, pp. 156–171.
[27] Pearson, S. R., and Shipway, P. H., 2015, "Is the Wear Coefficient Dependent Upon Slip Amplitude in Fretting? Vingsbo and Söderberg Revisited," Wear, **330–331**, pp. 93–102.
[28] Yu, S. R., Bai, L. R., Jin, P. F., and Song, W., 2018, "Effect of Counterpart Materials on Fretting Wear Behavior of TC4 Titanium Alloy," Lubr. Eng., **43**(8), pp. 14–18.
[29] Kang, J., Wang, M., Yue, W., Fu, Z., Zhu, L., She, D., and Wang, C., 2019, "Tribological Behavior of Titanium Alloy Treated by Nitriding and Surface Texturing Composite Technology," Materials, **12**(2).
[30] Ding, H. H., Fridrici, V., Geringer, J., Fontaine, J., and Kapsa, P., 2019, "Low-Friction Study Between Diamond-Like Carbon Coating and Ti6Al4V Under Fretting Conditions," Tribol. Int., **135**, pp. 368–388.
[31] Zhang, X. Y., Cai, Z. B., Peng, J. F., Liu, J. H., and Ren, P. D., 2018, "Experimental Study of the Fretting Wear Behavior of Inconel 690 Alloy Under Alternating Load Conditions," Proc. Inst. Mech. Eng., Part J, **232**(11), pp. 1343–1351.